

See discussions, stats, and author profiles for this publication at: <https://www.researchgate.net/publication/260430891>

Molecular dynamics simulation of the phosphorylation-induced conformational changes of a tau peptide fragment

ARTICLE *in* PROTEINS STRUCTURE FUNCTION AND BIOINFORMATICS · SEPTEMBER 2014

Impact Factor: 2.63 · DOI: 10.1002/prot.24544 · Source: PubMed

CITATIONS

3

READS

58

3 AUTHORS, INCLUDING:



Neha S Gandhi

Curtin University

26 PUBLICATIONS 645 CITATIONS

SEE PROFILE

Molecular dynamics simulation of the phosphorylation-induced conformational changes of a tau peptide fragment

Albert J. Lyons, Neha S. Gandhi, and Ricardo L. Mancera*

School of Biomedical Sciences, CHIRI Biosciences, Curtin University, Perth 6845, Western Australia

Aggregation of the microtubule associated protein tau (MAPT) within neurons of the brain is the leading cause of tauopathies such as Alzheimer's disease. MAPT is a phospho-protein that is selectively phosphorylated by a number of kinases *in vivo* to perform its biological function. However, it may become pathogenically hyperphosphorylated, causing aggregation into paired helical filaments and neurofibrillary tangles. The phosphorylation induced conformational change on a peptide of MAPT (htau_{225–250}) was investigated by performing molecular dynamics simulations with different phosphorylation patterns of the peptide (pThr231 and/or pSer235) in different simulation conditions to determine the effect of ionic strength and phosphate charge. All phosphorylation patterns were found to disrupt a nascent terminal β -sheet pattern (²²⁶VAVVR²³⁰ and ²⁴⁴QTAPVP²⁴⁹), replacing it with a range of structures. The double pThr231/pSer235 phosphorylation pattern at experimental ionic strength resulted in the best agreement with NMR structural characterization, with the observation of a transient α -helix (²³⁹AKSRLQT²⁴⁵). PPII helical conformations were only found sporadically throughout the simulations.

Proteins 2014; 82:1907–1923.
© 2014 Wiley Periodicals, Inc.

Key words: tau protein; MAPT; microtubule; molecular dynamics; phosphorylation.

INTRODUCTION

Aggregation of the microtubule associated protein tau (MAPT) within neurons of the brain is the leading cause of tauopathies such as Alzheimer's disease. The tau protein polymerizes tubulin into microtubules (MTs) and stabilizes MTs within the neuron.¹ The tau protein is regulated by selective phosphorylation of amino acids preceding proline by proline-directed kinases such as GSK3 β and CDK2/CycA3, which acts as a selective “switching” mechanism to induce conformational changes.² There are a number of isoforms of the tau protein, with the principal component of protein aggregates in the diseased brain being hyperphosphorylated human tau₄₄₁ (htau₄₄₁), an isoform 441 residues long.

The htau₄₄₁ isoform consists of four conserved microtubule-binding repeats (MTRs-R1: Gln244-Lys274, R2: Val275-Ser305, R3: Val306-Gln336, and R4:Val337-Asn368)³ within the microtubule-binding domain (MBD) near the C-terminus, a C-terminal domain, a projection domain in the N-terminal region consisting of 2 inserts (I1: Gly45-Asp74 and I2: Asp74-Ala103) and a proline-rich region (PRR) connecting these domains (Fig. 1).⁴

The level of phosphorylation for regular neuronal function in a healthy brain has been quantitatively defined as 2–3 moles of phosphate per mole of htau₄₄₁.⁵

When the phosphate mole ratio is three times greater than this, htau₄₄₁ is said to be hyperphosphorylated.⁵ Hyperphosphorylation of the tau protein makes it unable to associate with MTs, causing instead deleterious self-aggregation and the formation of paired helical filaments (PHFs), leading to neurofibrillary tangles (NFTs).⁶ The key binding sites in the tau protein that mediate its interaction with MTs contain basic amino acid residues, suggesting that phosphorylation of neighboring residues can result in electrostatic interactions that may modify the conformation of the tau protein and prevent its association with MTs.⁷

The tau protein is an intrinsically disordered protein (IDP),⁸ characterized by its low content of secondary structure and a high level of conformational flexibility. This has prevented the determination of its structure by X-ray diffraction methods. Nuclear magnetic resonance (NMR) spectroscopy has nonetheless permitted the characterization of the conformations and dynamics of the

Additional Supporting Information may be found in the online version of this article.

*Correspondence to: School of Biomedical Sciences, CHIRI Biosciences, Curtin University, GPO Box U1987, Perth 6845, Western Australia.
E-mail: R.Mancera@curtin.edu.au

Received 15 December 2013; Revised 5 February 2014; Accepted 11 February 2014
Published online 27 February 2014 in Wiley Online Library (wileyonlinelibrary.com). DOI: 10.1002/prot.24544

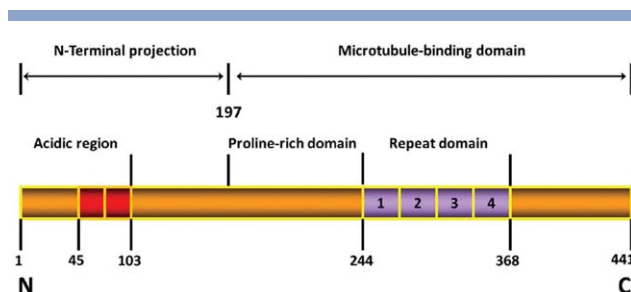


Figure 1

Full length htau₄₄₁ with two inserts shown in red and MTRs R1-R4 shown in purple and numbered as 1–4. The N-terminal projection domain and the MBD are visible but the C-terminal domain is not differentiated from the MBD. Image reproduced by permission of In Tech available at: <http://www.intechopen.com/books/understanding-alzheimer-s-disease/phosphorylation-of-tau-protein-associated-as-a-protective-mechanism-in-the-presence-of-toxic-c-termi>.

tau protein, including the complete backbone assignment of full length htau₄₄₁.⁹ Alpha carbon (C^α) chemical shifts confirm the absence of well-defined secondary structure domains, although a number of regions with transient secondary structure have been identified.⁹ Within the MTRs the motifs ²⁵⁶VKSKIG²⁶² (in R1), ²⁷⁴KVQIINKKLDL²⁸⁴ (in R2), ³⁰⁵SVQIVYKPVDL³¹⁵ (in R3), ³³⁶QVEVKSEKLD³⁴⁵ (in R4), and ³⁵¹QSKIGSL³⁵⁷ (in R4) have been identified to transiently adopt a β-structure, with the two motifs in R2 and R3 found to have the highest propensity.⁹ The R2 and R3 MTRs also contain the two aggregation-prone hexapeptides PHF6 and PHF6* (²⁷⁵VQIINK²⁸⁰ and ³⁰⁶VQIVYK³¹¹, respectively).¹⁰ Other types of transient structures have also been identified within htau₄₄₁, including transient α-helical structures between I2 and the PRR (¹¹⁴LEDEAAGHVT¹²³) and in immediate proximity to the C-terminus (⁴²⁸LADEVASLA⁴³⁷).

A region just before R1 in the PRR, the ²²⁴KKVAVVR²³⁰ motif, is found to adopt a β-structure 18% of the time,⁹ consistent with secondary structure predictions of a β-sheet for the ²²⁵KVAVVR²³⁰ stretch.¹¹ The ²²⁴KKVAVVR²³⁰ motif is important because MT assembly by the MTRs has been found to increase by a factor of 10 when this motif is part of the peptide that is assembling MTs.¹² This motif along with the ²⁴⁰KSRLQTAPV²⁴⁸ region act as one of the “jaws” of MT binding and locks on to the MT to correctly position it for assembly by the MTRs,⁷ interacting with the repeat regions through its two Lys and one Arg residues, which strengthens its MT association.¹²

There are a number of specific phosphorylation sites whose phosphorylation has a detrimental effect on the ability of htau₄₄₁ to bind to MTs. Two phosphorylation sites, Thr231 and Ser235, are important for phosphorylation-induced self-aggregation of htau₄₄₁.^{13,14} However, there has been some controversy as to the precise effect of their phosphorylation on the local conformation of the tau

protein. Early CD and NMR spectroscopy studies found that phosphorylation of Thr231 and Ser235 in the tau protein fragment Lys224-Lys240 led to the formation of a β-turn in the region Val229-pThr231.¹⁵ However, these measurements were carried out in aqueous solutions of trifluoroethanol, which is a hydrophobic solvent known to promote secondary structures in proteins, where stabilization of β-turns seems to be the predominant effect.¹⁶

Bielska and Zondlo investigated two peptide fragments of htau₄₄₁ (Val229-Ser238 and Val229-Arg242) and found that complete phosphorylation (the peptides have three and four phosphorylation sites, respectively) of both fragments increased the polyproline type II (PPII) helical propensity.¹⁷ However, the effect was considerably lesser in the longer peptide,¹⁷ which may suggest that it would be lesser still in even longer peptides and full length htau₄₄₁. The smaller peptide encompasses the ²³²PPKSPSSA²³⁹ motif, which has been found to transiently adopt a PPII helical conformation in its nonphosphorylated form in full length htau₄₄₁,⁹ suggesting that it possesses an intrinsic propensity that is necessary for phosphorylation-induced PPII formation.¹⁷ Increase in the ¹⁵N R_{1ρ} spin relaxation rates also indicated that full length htau₄₄₁ has increased rigidity in the range Ile151-Ser235, providing further evidence of stable PPII character in the absence of phosphorylation.⁹ A basic residue immediately preceding a phosphorylation site (which Thr231 and Ser235 are examples of) is a motif that will increase PPII character in nearby motifs upon phosphorylation.¹⁷ The observed increase in PPII content upon phosphorylation increased with increasing pH, confirming that electrostatic interactions are responsible for these conformational changes.¹⁷ The phosphorylated so-called TauF4 peptide (Ser208-Ser324) has also been determined to exhibit a PPII helix (²¹²TPSLPTPPTREPKKVAVVRTPPK²³⁵).¹³

Phosphorylation by the proline-directed CDK2/CycA3 kinase was found to strongly decrease the MT-binding ability of the TauF4 fragment and increase the α-helical propensity of a region just before the MBD (²³⁷SSAKSRLQ²⁴⁴).¹³ Specific phosphorylation of Thr231 and Ser235 exhibited an α-helical-stabilizing effect, suggesting that this effect is sequence specific; however, it was not possible to differentiate between the effects of individual phosphorylation of Thr231 and Ser235.¹³ Phosphorylation of Thr231 by the GSK3β proline-directed kinase has been found to be necessary to decrease MT binding, which is enhanced by the prior phosphorylation of Ser235.^{18,19} However, the sole phosphorylation of Thr231 by the CDK2/CycA3 proline-directed kinase has also been found to be sufficient to reduce the MT binding ability of the tau protein, while phosphorylation of Ser235 alone has been found to be irrelevant.²⁰ The content of secondary structure was found to change from 0.3% α-helix, 58.4% β-sheet and 0% helical turn prior to phosphorylation, to 28.5% α-helix, 0% β-sheet and 29.6% helical turn after phosphorylation.¹⁹

Table I

List of Systems Simulated: Op (Thr231 and Ser235), Tp (pThr231 and Ser235), Sp (Thr231 and pSer235), 2p (pThr231 and pSer235), i (Simulated Ionic Strength of 50 mM), t (Truncated), and (−2) (−2 Charge on Phosphates)

System	Phosphorylation pattern	Phosphate charge	Length	Solvent molecules
Op	No phosphorylation	N/A	K225-M250	3994
Tp	pT231	−1	K225-M250	3013
Sp	pS235	−1	K225-M250	3066
2p	pT231 and pS235	−1	K225-M250	3201
Opi	No phosphorylation	N/A	K225-M250	3986
Tpi	pT231	−1	K225-M250	3956
Spi	pS235	−1	K225-M250	3897
2pi	pT231 and pS235	−1	K225-M250	3972
Tpi(−2)	pT231	−2	K225-M250	3862
Spi(−2)	pS235	−2	K225-M250	3897
2pi(−2)	pT231 and pS235	−2	K225-M250	3974
Opit	No phosphorylation	N/A	P223-P247	4778
2pit	pT231&pS235	−1	P223-P247	4867

Molecular dynamics (MD) simulations have been used to characterize conformational changes to proteins and peptides upon phosphorylation. For example, stathmin and phospholamban exhibited the loss of α -helical content upon phosphorylation due to the disruption of native salt bridges and the formation of new salt bridges between the phosphorylated residues and other residues within the native α -helix.^{21,22} However, phosphorylation of the natively disordered N-terminal domain of smooth muscle myosin resulted in the stabilization of an α -helix due to the formation of a specific salt bridge.²³ It has indeed been hypothesized that phosphorylation of the N-terminus of α -helices leads to their stabilization through the creation of favorable electrostatic interactions.^{24,25} Similar interactions can indeed be found in the TauF4 peptide upon phosphorylation, where pThr231 and pSer235 create an N-cap with α -helical stabilizing properties.¹³

This study aims to shed further light on the effects of phosphorylation of Thr231 and Ser235 on the possible local conformation of htau₄₄₁ by carrying out a series of MD simulations of a 26-residue peptide defined as htau_{225–250} and a truncated 25 residue peptide defined as htau_{223–247}. These peptides contain these two critical phosphorylation sites, as well as adjacent regions containing a number of structural motifs that have been reported to be affected by phosphorylation.

MATERIALS AND METHODS

The htau_{225–250} fragment (²²⁵KVAVVRTPPKSPSSAKSRLQTAPVPM²⁵⁰) and the truncated version htau_{223–247} (²²³PKKVAVVRTPPKSPSSAKSRLQTAP²⁴⁷) were considered in their nonphosphorylated and phosphorylated forms (Table I). The htau_{225–250} fragment was chosen as it contains nearly the entire ²²⁴KKVAVVR²³⁰ motif, the phosphorylation sites Thr231 and Ser235, the ²³²PPKSPSSA²³⁹ motif, and a large

portion of the hydrophobic ²⁴⁵TAPVPMPDL²⁵³ motif from the R1 domain.

Phosphorylation of Thr231 has been found to be part of the recognition motif of Pin1, an isomerase that recognizes prolyl bonds in the *trans* conformation and catalyzes their isomerisation to the *cis* configuration.²⁶ All Pro residues in the peptides were thus constructed in the *trans* conformation.

Each peptide was placed within a 10 nm long cubic simulation box, and was then solvated with water. The different peptides simulated were all positively charged (between +5 and +3, depending on the system), with Cl[−] counter ions added to neutralize the charge. Different phosphorylation patterns were investigated by modifying the side chains of residues Thr231 and Ser235 (Table I).

Each peptide was initially energy minimized for 5000 steps of conjugate gradients by relaxing all water molecules and hydrogen atoms in the peptide, with the peptide backbone restrained with a force constant of 100 kcal/mol-Å². This same protocol was then repeated for another 5000 steps of minimization using conjugate gradients but with the backbone restraints relaxed to a force constant of 50 kcal/mol-Å². After this, a further 1000 steps of energy minimization were performed using conjugate gradients followed by 500 steps of steepest descents, in both cases with no restraints. These energy minimizations were performed using the AMBER 12 software package.²⁷

Once each peptide was fully energy minimized, 50 ps of MD equilibration in the NPT ensemble was undertaken at 1 atm and 310 K. To ensure that the peptide had no initial secondary structure that may bias the results, a vigorous simulated annealing protocol was then applied by heating the system to 400 K before cooling back down to 310 K over 10 ns in the NPT ensemble each way. Upon inspection, the peptide was then confirmed to be disordered after completely losing its entire initial secondary structure. To emulate the ionic strength

(50 mM) of the buffer used in the experimental conditions,¹³ four additional Na⁺ and Cl⁻ ions were added in most simulations (Table I).

All simulations were conducted using the AMBER 12 software package with the AMBER ff10 force field,^{28–30} which includes specific parameters for phosphorylated side chains, both with -1 and -2 charged phosphates (Table I).³¹ The TIP3P potential³² was used for water as this was the potential used in the parameterization of the phosphates.³¹ Electrostatic interactions were computed using the particle mesh Ewald method³³ using a fourth order spline for interpolation, and van der Waals interactions were computed using a cut-off of 10 Å. The time-step used in the simulations was 2 fs, with production runs conducted for 1.0 μ s total simulation time. During this period, coordinates were saved every 10 ps for subsequent analysis to determine changes in the secondary structure of the peptides, identify the most important conformations sampled by the peptides, and the formation of key intramolecular salt bridges. Hydrogen bond analysis was performed using AMBER Tools 1.3.²⁷

There is an inherent difficulty in the prediction of chemical shifts and J-couplings in IDPs and indeed coil regions in globular proteins.^{34,35} Consequently, no attempt was made to predict these NMR parameters directly from the simulation trajectories to compare with experiment. Instead, direct measurements of secondary structure content were performed.

To analyze the changes in the secondary structure of the peptides in each simulation, the Secondary Structure Assigning Mechanism within the Dictionary of Secondary Structure Program (DSSP)³⁶ was implemented in GRO-MACS.³⁷ DSSP assigns residues by hydrogen-bonded structure as either helical (3_{10} helix, α helix, π helix, or single helical turn, differentiated by backbone intrahelical hydrogen bonding patterns of the amine hydrogen “i” with the carbonyl oxygen “i + n”: i – i + 3, i – i + 4, and i – i + 5, or single hydrogen bond, respectively) or β structure (β bridges, which are isolated hydrogen-bonded structures, and β strands, which are contiguous bridges).³⁶ There is also one nonhydrogen bonded assignment of bend, which is a region of “high curvature”.³⁶ If a residue is not in a hydrogen bonded structure and has low curvature, it is assigned blank,³⁶ often interpreted as random coil. DSSP was used through the DSSP^{PPII} program to also determine the presence of PPII helical content on the basis of backbone hydrogen bonding distances, backbone ϕ and ψ dihedral angles and other factors.³⁸ Plots of the secondary structure content per residue over time were then generated for each simulation. The backbone ϕ and ψ dihedral angles were also used to construct Ramachandran plots for each residue of the peptides.

Clustering of the conformations sampled by the peptide in each simulation was done using the g_cluster analysis tool in GROMACS.³⁹ Due to the high conservation of

structural motifs in both termini in most simulations, these motifs were disregarded in the clustering analysis to prevent a systematic bias. The peptides in each simulation were thus clustered by considering only their central portion (the region ²³²PPKSPSSAKSRLQT²⁴⁵), using a 3.0 Å cut-off. The resulting cluster representative structures from each simulation were then clustered again, which in addition to visual inspection (using UCSF Chimera and structural alignment with the Matchmaker algorithm⁴⁰), allowed to determine the most appropriate list of consensus representative conformations across all simulations.

The presence of salt bridges within the peptide structure in each simulation was established using the Salt Bridges Plugin⁴¹ of the VMD molecular visualization software,⁴² which identified acidic and basic residues that came within a distance of 0.6 nm, the distance criterion set to define a salt bridge during the simulation.²¹ In addition, suitable representative structures of the most populated clusters were also analyzed to identify the predominant salt bridge interactions present.

RESULTS AND DISCUSSION

Simulations at zero ionic strength

The first set of simulations was conducted with the htau_{225–250} fragment at zero ionic strength with various phosphorylation states (0p, Tp, Sp, and 2p, as described in Table I). Figure 2 shows the DSSP^{PPII} plots along the simulation trajectory for each system as well as plots showing the average content of each type of secondary structure (measured by the percentage time sampled during the simulation) for each residue in the peptide.

In the case of the 0p simulation, the DSSP^{PPII} plot showed a very high propensity (almost the entire simulation) for β -strand conformation for the ²²⁶VAVVRT²³¹ and ²⁴⁴QTAPVP²⁴⁹ motifs [Fig. 2(a,b)]. This is in agreement with NMR characterization of full length htau₄₄₁ for the ²²⁶VAVVRT²³¹ motif (with the ²²⁴KKVAVVR²³⁰ motif found to have β structure 18% of the time),⁹ but not for ²⁴⁴QTAPVP²⁴⁹ (with formation of β structure for ²⁴³LQTAPVPMPDL²⁵³ hindered by the presence of the three Pro residues in full-length htau₄₄₁).⁹ However, this effect was lessened in the htau_{225–250} peptide as one of the Pro is not present. In addition, the motif is on the C-terminus and consequently has residues with unsatisfied H-bonding interactions that can find their partners by forming an anti-parallel β -sheet with the N-terminal β -strand, which can be seen to form by molecular visualization of simulation trajectory of the peptide,⁴² consistent with both strands occurring concurrently in the DSSP^{PPII} plot, suggesting they are associating with each other. The stabilization of this C-terminal β -strand may thus emulate interactions with other β -strands not present in this peptide within the repeat domains of full length htau₄₄₁ (²⁵⁶VKSKIG²⁶², ²⁷⁴KVQIINKKLDL²⁸⁴,

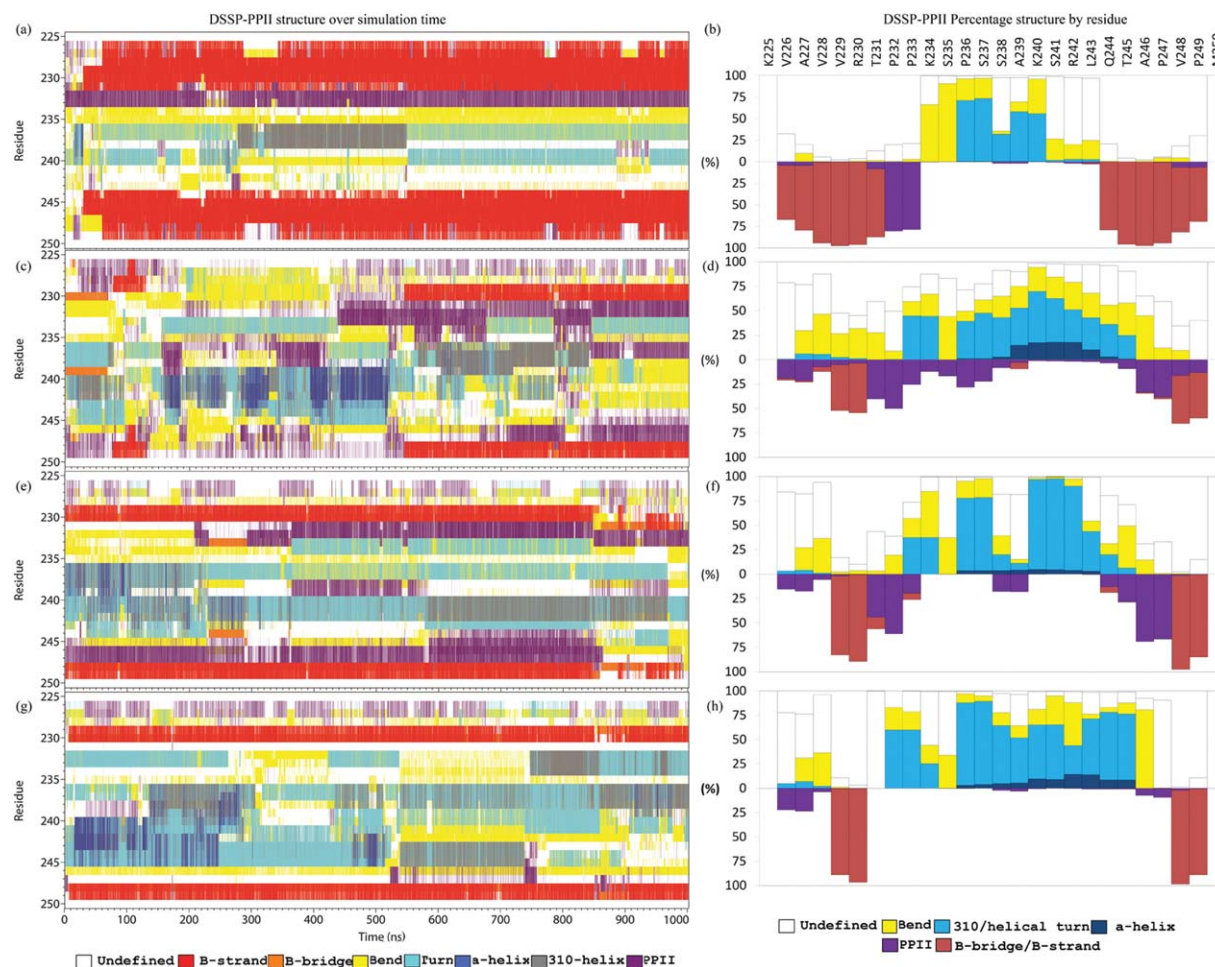


Figure 2

DSSP^{PPII} plots of secondary structure (colored as per legend) over simulation time - for simulations 0p (a), Tp (c), Sp (e), and 2p (g). Also shown are the bar charts for simulations 0p (b), Tp (d), Sp (f), and 2p (h), indicating the average percentage of secondary structure content per residue during the simulation. Helical turns and 3_{10} helices (cyan), α -helices (blue), bends (yellow), and undefined structures (white) are shown above the x-axis, whereas β (red) and PPII (purple) structures are shown below the x-axis of the bar chart. [Color figure can be viewed in the online issue, which is available at wileyonlinelibrary.com.]

³⁰⁵SVQIVYKPVDL³¹⁵, ³³⁶QVEVKSEKLD³⁴⁵ and ³⁵¹QSKIGSL³⁵⁷).⁹ One of these interactions of particular significance is that with the hexapeptide PHF6 (³⁰⁶VQIVYK³¹¹) motif,⁴³ known to form into a β -strand and precede aggregation of the tau protein.⁴⁴ In the simulation of the htau_{225–250} fragment, interactions between the two termini would in turn help to stabilize the N-terminal β -strand, as it would otherwise occur in full length htau₄₄₁.

All of the phosphorylation patterns investigated abolished the above 6-residue long β -strands but consistently maintained two residues in a vestigial β -strand conformation near each terminus (²²⁹VR²³⁰ and ²⁴⁸VP²⁴⁹), which once again associate with each other in an antiparallel fashion for most of the time in most simulations.

The Tp simulation exhibited a region with 10–18% α -helical propensity (²³⁹AKSRL²⁴³), in agreement with the

NMR characterization of this part of the phosphorylated tau protein,^{13,20} and in further agreement with suggestions that phosphorylation of Thr231 is primarily responsible for phosphorylation-induced conformational changes of the tau protein and that Ser235 phosphorylation alone is not sufficient.²⁰ Formation of the terminal vestigial β -strands seems to be anticorrelated with the formation of the intervening α -helical structure [Fig. 2(c)]. The Tp simulation also exhibits transient PPII helical conformations. The longest stretch (²³¹TPPKSPSS²³⁸) was observed 8–50% of the time [Fig. 2(d)]. The Sp and 2p simulations had similar structures, both containing an initial weakly defined transient α -helical region, the terminal anti-parallel vestigial β -strands and intervening interspersed bends and helical turns for the entire simulation time [Fig. 2(e,g)]. One of the major differences between these two systems is that the Sp simulation had

significant (but not extensive) PPII helical content throughout the simulation [Fig. 2(e)], rivaling the Tp simulation [Fig. 2(c)] and even exceeding it for some small stretches ($^{232}\text{PP}^{233}$ and $^{246}\text{AP}^{247}$).

The 2p simulation had the vestigial near terminal 2-residue β -strands clearly defined (near 100%) [Fig. 2(h)], as described earlier. However, it did not exhibit any significant PPII helical propensity. Furthermore, while there were substantial and consistent helical structures (such as 3–10 helix and helical turns) in the $^{232}\text{PKSPSSA}^{239}$ region, there was limited α -helical content in the adjacent $^{239}\text{AKSRLQT}^{245}$ region.

These simulations suggest that, at zero ionic strength, htau_{225–250} has terminal β -sheet propensity which is abolished upon phosphorylation (pThr231 and/or pSer235). This effect is accompanied by a limited increase in α -helical propensity in the region $^{239}\text{AKSRL}^{243}$, and more general PPII helicity throughout, particularly in the vicinity of Pro residues). However, upon full phosphorylation, there is loss of PPII helical content and a reduction in α -helical propensity, which is not consistent with NMR determinations carried out at high ionic strength.¹³

Simulations at 50 mM ionic strength

Simulations of all four phosphorylation patterns of the same htau_{225–250} fragment were repeated at 50 mM ionic strength (with 4 Na^+Cl^- ions; 0pi, Tpi, Spi, and 2pi, as described in Table I). The conformational preferences of the peptide in each system are displayed by DSSP^{PPII} plots over time and average percentage per residue in Figure 3.

The 0pi simulation has a striking similarity to the 0p simulation. Both simulations reveal the same secondary structure pattern of an N-terminal six residue long β -strand ($^{226}\text{VAVVRT}^{231}$) in an anti-parallel association with a C-terminal six residue long β -strand ($^{244}\text{QTAPVP}^{249}$) [Fig. 3(a,b)]. This is to be expected as the addition of charged ions will primarily affect electrostatic interactions, which the nonphosphorylated peptide lacks.

All the phosphorylation patterns investigated abolished the six residue long N- and C-terminal β -strands, but gave rise to secondary structure profile different to the zero ionic strength simulations. The transient PPII and α -helical structures observed in the Tp simulation are nearly absent in the Tpi simulation, with only a consistent pattern in the $^{231}\text{TPPKSPSSA}^{239}$ region consisting of bends, helical turns and undefined structures bounded by β -bridges, present for almost the entire simulation [Fig. 3(c)]. The vestigial β -strand structure $^{229}\text{VR}^{230}$ in the Tp simulation becomes more extended to the $^{226}\text{VAVVR}^{230}$ region, whereas the vestigial β -strand $^{248}\text{VP}^{249}$ remains unchanged.

In the Spi and 2pi simulations, both the $^{229}\text{VR}^{230}$ and $^{248}\text{VP}^{249}$ vestigial β -strands were formed again, present

for nearly the entire simulation length [Fig. 3(e,g)]. The Spi simulation exhibited in addition a consistent range of undefined coil, bends and 3–10 helical turns in the $^{234}\text{KSPSSAKSRLA}^{246}$ region, but unlike the Sp simulation there were no significant PPII or α -helical secondary structures.

As in the case of the 2p simulation, the 2pi simulation exhibited consistent helical structures (such as 3–10 helix and helical turns) in the $^{232}\text{PKSPSSA}^{239}$ region, but in this case, there was a strong α -helix in the adjacent $^{239}\text{AKSRLQT}^{245}$ region during approximately one third of the simulation [Fig. 3(g)]. The presence of this α -helix is in somewhat better agreement with NMR determinations for the TauF4 peptide, which were carried out for this phosphorylation pattern at an equivalent ionic strength.¹³ The PPII helical character of the entire peptide across all phosphorylation patterns was greatly decreased in the simulations at 50 mM ionic strength compared with simulations at zero ionic strength.

The simulations at 50 mM ionic strength reveal that the htau_{225–250} has terminal β -sheet propensity which tends to be abolished upon phosphorylation (pThr231 and/or pSer235). While this effect is also observed in simulations at zero ionic strength, the presence of an ionic strength gives rise to a large α -helical propensity in the region $^{239}\text{AKSRL}^{243}$ upon double phosphorylation, which is in excellent agreement with NMR determinations.¹³ On the other hand, there was limited PPII helical content in the $^{231}\text{TPPKSPSSAK}^{240}$ region in the 2pi simulation, which is also consistent with NMR determinations.¹³

Simulations at 50 mM ionic strength with –2 charged phosphates

The simulations for all the phosphorylated peptides were repeated with –2 charged phosphates to emulate a higher pH and further investigate the electrostatic effect of magnitude of the charge upon phosphorylation on the structure of the peptide [Tpi(–2), Spi(–2), and 2pi(–2)], as described in Table I. Figure 4 reveals the conformational preferences of the peptide in each system as shown by DSSP^{PPII} plots over time and average percentage per residue.

The Tpi(–2) simulation exhibited for more than half of the simulation time, the same conformation in the $^{231}\text{TPPKSPSSA}^{239}$ region that was observed to persist for the entire Tpi simulation (consisting of bends, helical turns and undefined structures, bounded by β -bridges). In addition a weak transient PPII helix was formed in the $^{240}\text{KSRLQTAPVP}^{249}$ region that was not observed in the Tpi simulation, but which was replaced, along with the structures in the $^{231}\text{TPPKSPSSA}^{239}$ region, after 550 ns by two different structures: a helical pattern consisting of a transient 3_{10} helix ($^{232}\text{PPK}^{234}$) interconverting to a weak α -helix ($^{231}\text{TPPK}^{234}$), and a more stable α -helix ($^{236}\text{PSSAK}^{240}$). In general PPII helical content

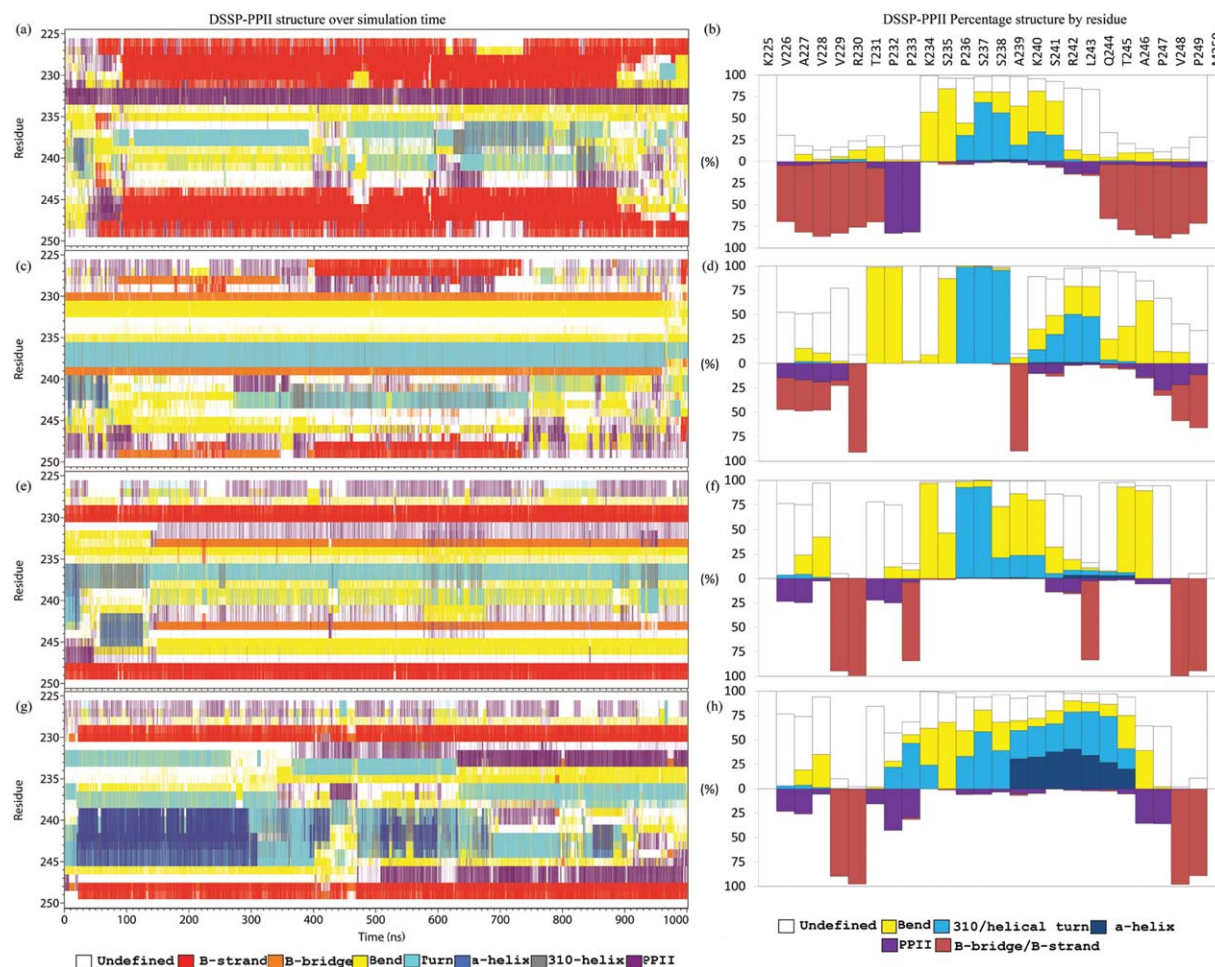


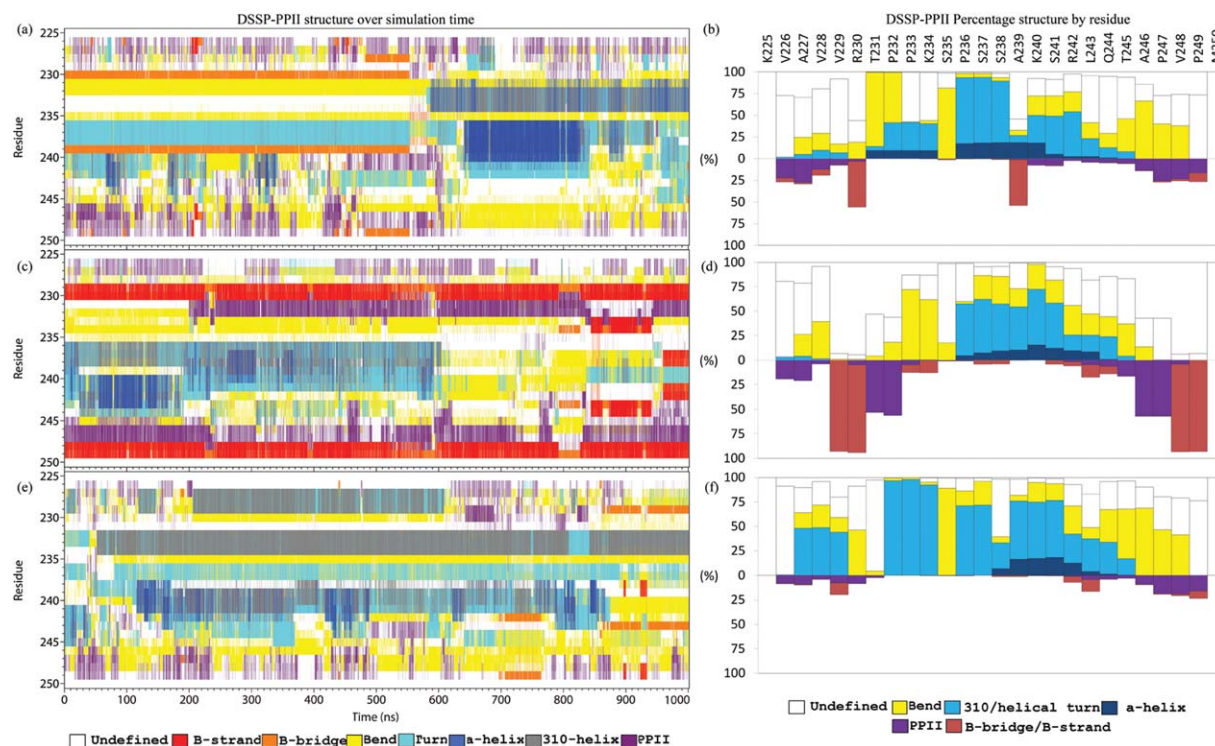
Figure 3

DSSP^{PPII} plots of secondary structure (colored as per legend) over simulation time—for simulations 0pi (a), Tpi (c), Spi (e), and 2pi (g). In addition, shown are the bar charts for simulations 0pi (b), Tpi (d), Spi (f), and 2pi (h), indicating the average percentage of secondary structure content per residue during the simulation. Helical turns and 3_{10} helices (cyan), α -helices (blue), bends (yellow), and undefined structures (white) are shown above the x-axis, whereas β (red) and PPII (purple) structures are shown below the x-axis of the bar chart. [Color figure can be viewed in the online issue, which is available at www.interscience.wiley.com.]

appears to be greatly reduced in the Tpi(−2) and 2pi(−2) simulations [Fig. 4(b,f)]. However, the PPII helical structures in the N and C termini (²²⁶VAVV²²⁹ and ²⁴⁶APVP²⁴⁹, respectively) in the Tpi(−2) simulation and in the C-terminus (²⁴⁶APVP²⁴⁹) of the 2pi(−2) simulation remain throughout the entire trajectory, albeit transiently. Therefore, changes in the net charge of the phosphates do not appear to result in large overall changes in the PPII helical content at the termini of the peptide. It is important to note that the PPII helical conformations observed in the TauF4 peptide were longer because this peptide stretched out beyond the limits of htau_{225–250}, which is likely to increase the extent of this conformation.

The most pertinent difference caused by the increased charge on the phosphate groups is the increase in α -helical propensity across all phosphorylation patterns: the already mentioned α -helix in Tpi(−2) as well as in

Spi(−2), and 2pi(−2) in the ²³⁸AKSRL²⁴³ region. This is consistent with the 2pi simulation described above and with NMR data¹³; however, the α -helical content appears to be more transient, interconverting to helical turns and 3_{10} helices. Hence, while increase in the charge of the phosphate groups increases the helical propensity of the peptide in all phosphorylation patterns, the resulting α -helix, especially in the 2pi(−2) simulation (the phosphorylation pattern that produced the strongest α -helix with the −1 charged phosphates), does not appear to have the same stability. This indicates that the role of the electrostatic interactions of the phosphate groups in modifying the α -helical propensity of the peptide is complex in nature. It is interesting to note that the protonated OH group in the phosphate of pThr231 in the 2pi simulation (with a charge of −1) formed a hydrogen bond with the backbone carbonyl of pSer235, an

**Figure 4**

DSSP^{PPII} plots of secondary structure (colored as per legend) over simulation time—for simulations Tpi-2 (a), Spi-2 (c), and 2pi-2 (e). In addition, shown are the bar charts for simulations Tpi-2 (b), Spi-2 (d), and 2pi-2 (f), indicating the average percentage of secondary structure content per residue during the simulation. Helical turns and 3_{10} helices (cyan), α -helices (blue), bends (yellow), and undefined structures (white) are shown above the x-axis, whereas β (red) and PPII (purple) structures are shown below the x-axis of the bar chart. [Color figure can be viewed in the online issue, which is available at wileyonlinelibrary.com.]

interaction that was observed for 11% of the simulation time and exclusively in the α -helical conformation. The peptide in the 2pi(-2) simulation, which has phosphate groups completely ionized, cannot form this interaction. This interaction may play role in the difference in stability of the α -helical region observed between the 2pi and 2pi(-2) simulations.

Another major difference is the complete loss of the vestigial β -strands in the Tpi(-2) and 2pi(-2) simulations. By contrast, the Spi(-2) simulation retains the same two terminal vestigial β -strands that have been persistent through the various phosphorylation patterns and has a higher proportion of PPII helical content, including the $^{226}\text{VAV}^{228}$ and $^{231}\text{TP}^{232}$ regions interspersed with the N-terminal vestigial β -strand ($^{229}\text{VR}^{230}$), as well as the $^{245}\text{TAP}^{247}$ region immediately preceding the C-terminal vestigial β -strand ($^{248}\text{VP}^{249}$).

Simulations of a truncated peptide at 50 mM ionic strength

The truncated peptide (htau_{223–247}) was investigated to establish the role of the C-terminus of the htau_{225–250} peptide on the conformation of the N-terminus. These

simulations were carried out for the nonphosphorylated and doubly phosphorylated peptide (0pit and 2pit respectively, as described in Table I). The conformational preferences of the peptide in each system as shown by DSSP^{PPII} plots over time and average percentage per residue are displayed in Figure 5.

The N-terminal β -strand observed in the nonphosphorylated htau_{225–250} peptide (0pi simulation) was also observed in the nonphosphorylated truncated htau_{223–247} peptide (0pit simulation), in agreement with NMR studies showing a tendency for β -strand formation of the $^{225}\text{KVA}^{230}\text{VR}^{230}$ motif,⁹ even though this motif was no longer on the N-terminus. However, it did still interact in an anti-parallel arrangement with a β -strand on the C-terminus ($^{241}\text{SRLQTA}^{246}$). This indicates that the $^{225}\text{KVA}^{230}\text{VR}^{230}$ motif has an intrinsic propensity to adopt a β -strand conformation that is induced by interactions with another β -strand elsewhere in the MTRs. This β -strand was, however, not present for roughly the first half of the simulation, where instead a transient PPII helical structure was observed in the $^{224}\text{KKVAVVRTPPKSPS}^{237}$ region, which is in agreement with reports of PPII helical content in the $^{232}\text{PPKSPSSA}^{239}$ motif of full length nonphosphorylated

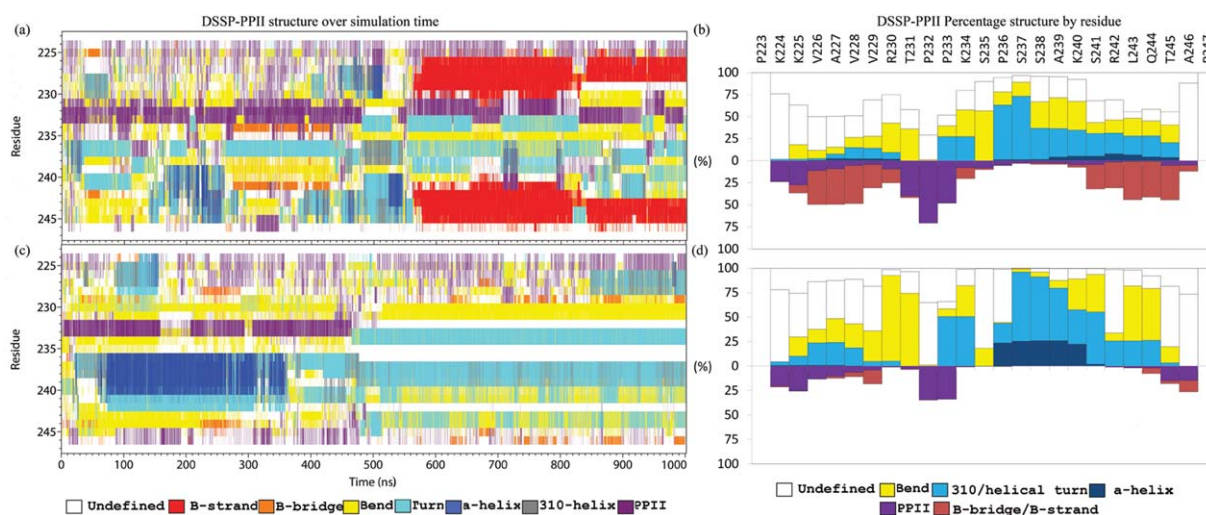


Figure 5

DSSP^{PPII} plots of secondary structure (colored as per legend) over simulation time—for simulations 0pit (a) and 2pit (c). In addition, shown are the bar charts for simulations 0pit (b) and 2pit (d), indicating the average percentage of secondary structure content per residue during the simulation. Helical turns and 3_{10} helices (cyan), α -helices (blue), bends (yellow), and undefined structures (white) are shown above the x-axis, whereas β (red) and PPII (purple) structures are shown below the x-axis of the bar chart. [Color figure can be viewed in the online issue, which is available at wileyonlinelibrary.com.]

htau₄₄₁,⁹ As with the htau_{225–250} peptide, the α -helical content of the nonphosphorylated peptide was minimal. The rest of the peptide structure was comprised mostly of a mix of bends, coils, and helical turns.

The 2pit simulation showed the formation of a transient α -helix in the ²³⁶PSSAK²⁴⁰ region, which is a somewhat shorter region that appears earlier in the sequence compared to the ²³⁹AKSRLQT²⁴⁵ α -helical region seen in the 2pi simulation. Both simulations show the best agreement with NMR data, which shows an increase in the α -helical propensity of the ²³⁵SPSSAKSRLQ²⁴⁴ region in the TauF4 fragment.¹³

Finally, the terminal vestigial β -strands were completely absent in the 2pit simulation, indicating that their presence in the phosphorylated htau_{225–250} peptides was due to the ²²⁵KVAVVR²³⁰ motif being at the N-terminus in combination with its intrinsic β propensity, leading to the presence of unsatisfied hydrogen bonds that drive the interaction with the antiparallel β -strand at the C-terminus. The same transient N-terminal PPII region (²²⁴KKVAVVRTPP²³³) seen in the 0pit simulation was present, suggesting that its formation is independent of phosphorylation. However, this increase in PPII helical propensity did not extend to the ²³²PPKSPSSA²³⁹ motif, as reported by NMR studies upon phosphorylation.¹⁷

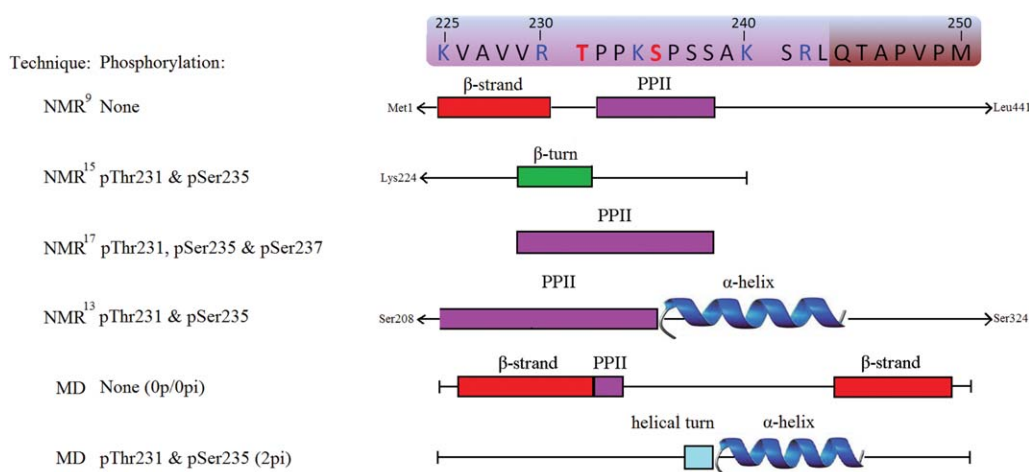
Optimum simulation conditions to investigate the htau_{225–250} fragment

The DSSP^{PPII} structure plots of htau_{225–250} (Figs. 2–5) reveal the presence of various transient secondary structures

during all simulations, in agreement with the reorientation of secondary structures in IDPs in the low-ns timescale.⁴⁵ The backbone conformations of most amino acids in the peptide thus populated a range of secondary structure values. The Ramachandran plots for each amino acid of the peptide in all simulations can be found in the Supporting Information (Figs. S1–S13). Restricted mobility and stability of secondary structure elements in IDPs however, is often correlated with the presence of binding sites in IDPs.⁴⁵ This may explain why the ²²⁵KVAVVR²⁵⁰ motif is such a stable structure, since it is a MT-binding site of the tau protein.

The same simulations were conducted in different conditions (no ionic strength and 50 mM ionic strength with -1 or -2 charged phosphates). As expected, the 0p simulation with no ionic strength for the nonphosphorylated peptide gave comparable results to the 0pi simulation including ionic strength. This was due to the limited effect of ions in a system without charged phosphates. Both simulations reproduced experimental NMR data for the ²²⁵KVAVVR²³⁰ motif, showing a β -strand, but did not show appreciable PPII content aside from the ²³²PP²³³ motif, which the NMR experiments do indicate.⁹ In the case of the phosphorylated peptides, simulations at the experimental ionic strength led to significant changes to the conformational preferences of the peptides due to the effects of electrostatic screening of the added ions.

The effect of phosphorylation was investigated using the two charged states of the phosphate groups (-1 and -2). The simulations reveal that the presence of -1 charged phosphate groups result in the best agreement with experiment. This suggests that the electrostatic

**Figure 6**

Graphical representation of the experimental determinations for htau_{225–250} and its comparison with the MD simulation studies presented in this work. [Color figure can be viewed in the online issue, which is available at wileyonlinelibrary.com.]

interactions that are responsible for modifying the conformation of the peptide are sensitive to the magnitude of the charge.

The simulations of the nonphosphorylated peptide confirm that the ²²⁵KVAVVR²³⁰ motif has an intrinsic tendency to adopt a transient β -strand conformation, in which the basic Lys225 and Arg230 residues are exposed to the solvent, supporting the notion that they are free to interact with the MTs in the full length tau protein. All simulations revealed that phosphorylation abolished this β -strand conformation (with the best agreement to NMR determination being the phosphorylated peptide in the 2pi simulation). A summary of the predicted conformational preferences of the htau_{225–250} peptide in its phosphorylated and non-phosphorylated forms is given in Figure 6, along with the findings of various NMR experiments.

Electrostatic interactions and conformational preferences

The htau_{225–250} peptide has a number of basic residues but no acidic residues, providing an opportunity

for the formation of electrostatic interactions upon addition of negatively charged phosphate groups through which its conformation can be affected. These interactions were investigated in detail by monitoring the salt bridges formed throughout the peptide over the course of all simulations (Table II). The consensus conformations of the peptides identified over all simulations are presented in Table III, while Table IV presents the non-consensus (unique) conformations identified in several of the simulations. Many of these preferred conformations are stabilized by salt bridge interactions.

The top most populated consensus conformation (Conformation 1, Table III) contained the α -helical conformation that has been identified by NMR analysis of the phosphorylated TauF4 peptide.¹³ The pThr231-Arg242 salt bridge was present in almost all of the simulations that exhibited the α -helical pattern, especially in the ²³⁹AKSRLQT²⁴⁵ range in the 2pi simulation, with formation of this salt bridge stabilizing the α -helical structure. Figure 7 shows a representative snapshot from the 2pi simulation with the salt bridges formed by Arg242 within the α -helix, showing both pThr231 and

Table II

List of Salt Bridges Formed in the htau_{225–250} Peptide and the Percentage Time of Their Occurrence During the Simulations

Simulation	pT-K225	pT-R230	pT-K234	pT-K240	pT-R242	pS-K225	pS-R230	pS-K234	pS-K240	pS-R242
Tp	3	16		13	6					
Sp								36		22
2p	3	5	21	13	30		20	10		13
Tpi		8		88						
Spi								36		27
2pi				6	60			35	4	22
Tpi(–2)		68	14	58	7					
Spi(–2)								48	5	60
2pi(–2)	44	21	88	3	14	3	76		14	92

Table III

Consensus Conformations Across all Simulations















Simulation	Consensus conformation 1	Consensus conformation 2	Consensus conformation 3	Consensus conformation 4
0p				
			97%	
Tp				
		9%		40%
Sp				
	6%			92%
2p				
	96%			
0pi				
			87%	
Tpi				
		86%		
Spi				
	5%		95%	
2pi				
	83%			
Tpi(-2)				
	36%	44%		
Spi(-2)				
	64%			

Table III
(Continued)






Simulation	Consensus conformation 1	Consensus conformation 2	Consensus conformation 3	Consensus conformation 4
2pi(-2)				
	84%			
0pit				
			28%	
2pit				
	24%			
Simulation	Consensus conformation 5	Consensus conformation 6	Consensus conformation 7	Consensus conformation 8
0p				
Tp				
		15%	3%	
Sp				
			1%	
2p				
0pi				
	6%			
Tpi				
				10%
Spi				
2pi				
		5%		

Table III
(Continued)

Simulation	Consensus conformation 5	Consensus conformation 6	Consensus conformation 7	Consensus conformation 8
Tpi(−2)				
				3%
Sp(−2)				
	29%			
2pi(−2)				
0pit				
2pit				

Each conformation is shown in a ribbon representation of the backbone of the peptide, with the N-terminus indicated by an asterisk. The percentage of the simulation time during which each conformation is sampled is included. [Color table can be viewed in the online issue, which is available at wileyonlinelibrary.com.]

pSer235 contributing to the stabilization of this conformation by forming salt bridges. This rationalizes why the three most populated clusters within Conformation 1 are all double phosphorylated peptides (pThr231 and pSer235), providing confirmation of the importance of this phosphorylation pattern in those experiments.¹³

Although Conformation 1 was sampled consistently by the peptide across most simulations, there is a shift in this conformational preference depending on the phosphorylation pattern and simulation conditions, which is reflected by the relative abundance of the conformation, as well as the specific form of the conformation, which ranged from disconnected helical turns to a full, well balanced α -helix. Of the three double phosphorylated peptides with the highest percentage, the 2p and 2pi peptides (with −1 charged phosphates) exhibited well formed α -helices, whereas the 2pi(−2) conformation exhibited disconnected helical turns. This is consistent with the destabilization caused by the extra charge in the 2pi(−2) simulation already discussed, and the inability of the pThr231 phosphate O to form a hydrogen bond with the pSer235 backbone, since it is not protonated. The sole representative of the pThr231 peptides in this conformation was moderately sampled in the Tpi-2 simulation (36%), whereas the pSer235 peptides were generally quite lowly sampled (6 and 5% in the Sp and Spi simulations, respectively) except for the Spi(−2) simulation (64%). However, as can be seen by examining the conformation shown in Table III, and in Figure 4(c), although well sampled, this conformation is not the full stable α -helix of the double phosphorylated peptide runs, but rather a single helical turn with the rest being a coil following the helical shape. This suggests that for sole Ser235 phosphorylation, an increase in phosphate

charge stabilizes a different but similar helical pattern. This is consistent with the effects of the phosphorylation pattern and simulation conditions discussed above.

The second most populated consensus conformation (Conformation 2, Table III) was found only in pThr simulations, with formation of the pThr231-Lys240 salt bridge being exclusively associated with the formation of this structure in the ²³¹TPPKSPSSA²³⁹ region. It is found entirely in the Tpi simulation and partially in the Tpi(−2) simulation, as already discussed (Fig. 8). The only simulations in which this salt bridge occurred appreciably were Tp (9%), Tpi (86%) and Tpi(−2) (44%), where it was present within the ²³¹TPPKSPSSA²³⁹ motif exclusively when the peptide was in the well-defined structure, reflected by the matching percentages of this salt bridge (Table II) with the structure propensity, especially for the Tpi and Tpi(−2) simulations [Figs. 3(c) and 4(a)]. Changes in the proportion of this conformation suggest that the electrostatic screening effect of the solvent ionic strength in the Tpi and Tpi(−2) simulations may have facilitated the formation of this salt bridge interaction, which appears to stabilize this conformation. This is a noteworthy conformation as the ²²⁵KVAVVR²³⁰ motif is stretched out and would be thus available to interact with MTs, hence confirming that sole Thr231 phosphorylation is not sufficient to induce a conformational change that can inhibit MT binding for the −1 charged phosphate. However, the two helical structures that form in the later parts of the Tpi-2 simulation (α -helix at ²³⁶PSSAK²⁴⁰ and $\alpha/3_{10}$ -helix at ²³²PPK²³⁴) are sampled in Conformation 1 and are stabilized by a salt bridge interaction with pThr231. Although the absence of the second phosphate prevents stronger stabilization, resulting in a conformation containing two

Table IV
Nonconsensus Conformations Across all Simulations

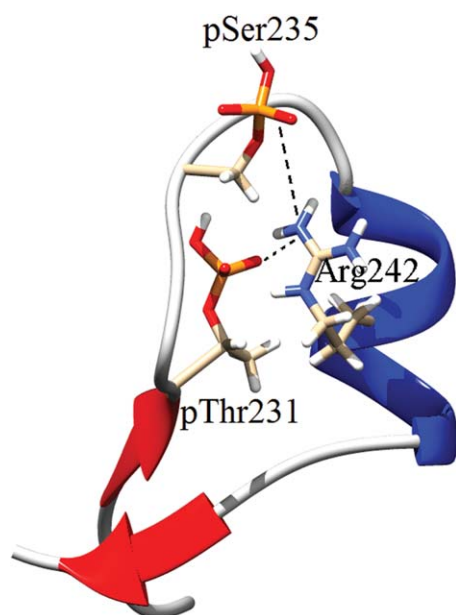
Simulation	Nonconsensus conformations			
0p				
Tp	 10%	 15%		
Sp				
2p				
0pi	 3%			
Tpi	 3%			
Spi				
2pi	 9%			
Tpi(−2)	 6%	 6%		
Spi(−2)	 5%			
2pi(−2)	 3%			
0pit	 19%	 16%	 12%	 4%
2pit	 67%	 4%		

Conformations are listed for each simulation but their position in the columns does not indicate any similarity.

smaller helical regions rather than a longer α -helix, the ²²⁵KVAVVR²³⁰ motif would remain unavailable for MT binding due to this conformational change.

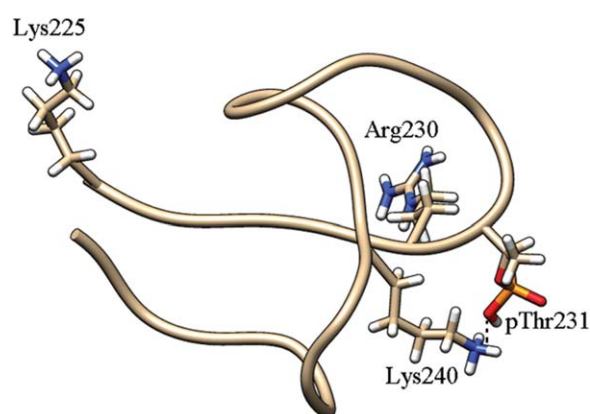
The third most populated consensus conformation (Conformation 3, Table III) was found in the nonphosphorylated peptide simulations (0p, 0pit, and 0pi), as well

as in the Spi simulation. This was the primary conformation of the Spi peptide (95%), as well as in the nonphosphorylated peptides (97, 87, and 28% for the 0p, 0pi, and 0pit simulations, respectively). This suggests that sole Ser235 phosphorylation does not affect the conformation of the peptide in a meaningful way. It is important to note

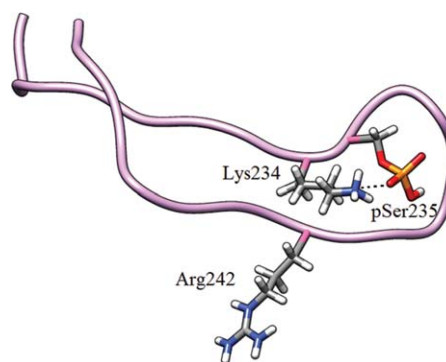
**Figure 7**

Snapshot (43.12 ns) from the 2pi simulation showing the α -helix and two salt bridge interactions (pThr231-Arg242 and pSer235-Arg242). The occurrence of the pThr231-Arg242 salt bridge interaction is correlated with the formation of the α -helix. [Color figure can be viewed in the online issue, which is available at wileyonlinelibrary.com.]

though that, in the case of the Spi simulation, the peptide has a similar conformation, aside from a kink around pSer235, which is caused by the salt bridges between pSer235 and both Lys234 and Arg242. The most dominant of these interactions can be seen in Figure 9. However, this interaction appears to be insufficient to cause any more

**Figure 8**

Snapshot (703.84 ns) from the Tpi simulation representing consensus conformation 2. The stabilizing salt bridge (pThr231-Arg240) is visible as a dashed line. The basic residues Lys225 and Arg230 (the start and end of the $^{225}\text{KVAVVR}^{230}$ motif) are accessible on the surface and may thus be able to interact with the MT. [Color figure can be viewed in the online issue, which is available at wileyonlinelibrary.com.]

**Figure 9**

Snapshot (266.28 ns) from the Spi simulation representing the most populated conformation (consensus conformation 3). The two basic residues (Lys234 and Arg242) that interact with pSer235 are shown as sticks. The most prominent salt bridge with Lys234 is visible as a dashed line. [Color figure can be viewed in the online issue, which is available at wileyonlinelibrary.com.]

than a minor kink in the structure of the peptide when compared with the nonphosphorylated conformations.

Conformation 4 (Table III) does not appear to have biological relevance (i.e., phosphorylation-induced conformational changes), as it was found only in simulations carried out at zero ionic strength (supporting the notion that this is not appropriate to characterize this fragment), specifically in the Tp (40%) and Sp (92%) simulations, again supporting the notion that sole Ser235 phosphorylation does not induce conformational changes of biological importance.

The remaining consensus conformations reported in Table III correspond to structures without significant defined secondary structure and not highly sampled (1–15%). Hence, these conformations do not appear to be significant for the understanding of the biologically relevant dynamics of the htau_{225–250} peptide.

There were a number of important nonconsensus (unique) conformations identified in several simulations (Table IV). Of particular significance is the highly populated conformation sampled in the 2pit simulation (67%). Table II reveals that a wide variety of different salt bridge interactions were formed during this simulation, suggesting the presence of a fine balance between this conformation and, for example, the dominant (and biologically relevant) conformation found in all other double-phosphorylated peptide simulations (Conformation 1). However, this conformation contained a single α -helical turn that disrupted the $^{225}\text{KVAVVR}^{230}$ motif, which could be speculated to affect MT binding as expected. In the 0pit simulation, the peptide exhibited a number of unique conformations and only one consensus conformation (it is most populated conformation, 28%). This was likely because the peptide had neither the effect of the terminal $^{225}\text{KVAVVR}^{230}$ antiparallel

β -sheet, nor any phosphate groups to provide stabilizing salt bridge interactions. Another interesting nonconsensus conformation from the nontruncated peptide was the second conformation shown in Table IV for the Tp simulation (populated 15% of the time). This conformation contains a well-defined α -helix ($^{239}\text{AKSRLQT}^{245}$) but was not clustered with the other helical conformations. While this conformation contains the stabilizing pThr231-Arg242 salt bridge, as found in consensus Conformation 1 (Table III), the peptide adopts an overall different conformation that does not exhibit interactions between the N- and C-termini.

CONCLUSIONS

MD simulations of the tau protein htau_{225–250} peptide confirm that phosphorylation is responsible for local disorder-to-order transitions that lead to the formation of more stable secondary structures. This process is driven by the formation of stabilizing electrostatic interactions (salt bridges) with the added phosphate groups.

The simulations conducted agree with NMR determination of this portion of full length htau₄₄₁,^{9,13} and provide further insight into the nature of the interactions involved in inducing conformational changes. In particular, the phosphorylation-induced increase in helical propensity of the htau_{225–250} peptide is most prominent at a 50 mM ionic strength with double phosphorylation of Thr231 and Ser235 and with -1 charged phosphate. However, PPII helical content of this peptide in all phosphorylation patterns and simulation conditions was found to be limited.

The $^{225}\text{KVAVVR}^{230}$ and $^{240}\text{KSRLQTAPV}^{248}$ motifs are known to strongly contribute to binding with the acidic outside of MTs.⁷ The simulations reported here have found that the N-terminal $^{226}\text{VAVVR}^{230}$ and C-terminal $^{244}\text{QTAPVP}^{249}$ regions form β -sheet patterns that indeed make them accessible to the solvent in the nonphosphorylated htau_{225–250}. Phosphorylation of the peptide was determined to lead to conformational changes due to the formation of salt bridges between the negatively charged pThr231/pSer235 residues and neighboring positively charged basic residues, disrupting the β -sheet patterns and thus rationalizing the hypothesis that these motifs become unavailable for binding to MTs. Consequently, the associated increases in PPII and helical propensity upon phosphorylation appear indeed to be an event that would favor the aggregation of the MAPT.

ACKNOWLEDGMENTS

The work was supported by iVEC through the use of advanced computing resources located at Epic @ Murdoch and Fornax @ UWA. The authors thank Prof. Guy Lippens for helpful discussions on experimental data of the TauF4 peptide. They acknowledge Cara Kreck for help with Perl scripting.

REFERENCES

- Weingarten MD. A protein factor essential for microtubule assembly. *Proc Natl Acad Sci USA* 1975;72:1858.
- Lu P-J, Wulf G, Zhou XZ, Davies P, Lu KP. The prolyl isomerase Pin1 restores the function of Alzheimer-associated phosphorylated tau protein. *Nature* 1999;399:784–788.
- Hiraoka S, Yao T-M, Minoura K, Tomoo K, Sumida M, Taniguchi T, Ishida T. Conformational transition state is responsible for assembly of microtubule-binding domain of tau protein. *Biochem Biophys Res Commun* 2004;315:659–663.
- Luna-Muñoz J, Harrington CR, Wischik CM, Flores-Rodríguez P, Avila J, Zamudio SR, Cruz FDI, Mena R, Meraz-Ríos MA, Floran-Garduño B. Phosphorylation of Tau Protein Associated as a Protective Mechanism in the Presence of Toxic, C-Terminally Truncated Tau in Alzheimer's Disease, Understanding Alzheimer's Disease, 2013, Prof. Inga Zerr (Ed.), ISBN: 978-953-51-1009-5, InTech, DOI: 10.5772/54228.
- Wang J-Z, Xia Y-Y, Grundke-Iqbal I, Iqbal K. Abnormal hyperphosphorylation of tau: sites, regulation, and molecular mechanism of neurofibrillary degeneration. *J Alzheimer's Dis* 2013;33:S123–S139.
- Ihara Y, Nukina N, Miura R, Ogawara M. Phosphorylated tau protein is integrated into paired helical filaments in Alzheimer's disease. *J Biochem* 1986;99:1807–1810.
- Mukrasch MD, von Bergen M, Biernat J, Fischer D, Griesinger C, Mandelkow E, Zweckstetter M. The “Jaws” of the Tau-Microtubule Interaction. *J Biol Chem* 2007;282:12230–12239.
- Tomba P. Structure and Function of Intrinsically Disordered Proteins. USA: CRC Press; 2010.
- Mukrasch MD, Bibow S, Korukottu J, Jeganathan S, Biernat J, Griesinger C, Mandelkow E, Zweckstetter M. Structural polymorphism of 441-residue tau at single residue resolution. *PLoS Biol* 2009;7:e1000034.
- von Bergen M, Barghorn S, Li L, Marx A, Biernat J, Mandelkow E-M, Mandelkow E. Mutations of tau protein in frontotemporal dementia promote aggregation of paired helical filaments by enhancing local β -structure. *J Biol Chem* 2001;276:48165–48174.
- Gamblin TC. Potential structure/function relationships of predicted secondary structural elements of tau. *Biochim Biophys Acta* 2005; 1739:140–149.
- Goode BL. Functional interactions between the proline-rich and repeat regions of tau enhance microtubule binding and assembly. *Mol Biol Cell* 1997;8:353.
- Sibille N, Huvent I, Fauquant C, Verdegem D, Amniai L, Leroy A, Wieruszkeski J-M, Lippens G, Landrieu I. Structural characterization by nuclear magnetic resonance of the impact of phosphorylation in the proline-rich region of the disordered Tau protein. *Proteins* 2012; 80:454–462.
- Hoffmann R, Lee VMY, Leight S, Varga I, Otvos L. Unique Alzheimer's disease paired helical filament specific epitopes involve double phosphorylation at specific sites†. *Biochemistry* 1997;36: 8114–8124.
- Daly NL. Role of phosphorylation in the conformation of τ peptides implicated in Alzheimer's disease. *Biochemistry* 2000;39:9039.
- Roccatano D, Colombo G, Fioroni M, Mark AE. Mechanism by which 2,2,2-trifluoroethanol/water mixtures stabilize secondary-structure formation in peptides: a molecular dynamics study. *Proc Natl Acad Sci* 2002;99:12179–12184.
- Bielska AA, Zondlo NJ. Hyperphosphorylation of tau induces local polypyrrolin II helix†. *Biochemistry* 2006;45:5527–5537.
- Cho J-H, Johnson GVV. Primed phosphorylation of tau at Thr231 by glycogen synthase kinase 3 β (GSK3 β) plays a critical role in regulating tau's ability to bind and stabilize microtubules. *J Neurochem* 2004;88:349–358.
- Lin Y-T, Cheng J-T, Liang L-C, Ko C-Y, Lo Y-K, Lu P-J. The binding and phosphorylation of Thr231 is critical for Tau's

- hyperphosphorylation and functional regulation by glycogen synthase kinase 3 β . *J Neurochem* 2007;103:802–813.
20. Amniai L, Lippens G, Landrieu I. Characterization of the AT180 epitope of phosphorylated Tau protein by a combined nuclear magnetic resonance and fluorescence spectroscopy approach. *Biochem Biophys Res Commun* 2011;412:743.
 21. Missimer JH, Steinmetz MO, van Gunsteren WF, Dolenc J. Influence of 63Ser phosphorylation and dephosphorylation on the structure of the stathmin helical nucleation sequence: a molecular dynamics study. *Biochemistry* 2012;51:8455.
 22. Germana Paterlini M, Thomas DD. The α -helical propensity of the cytoplasmic domain of phospholamban: a molecular dynamics simulation of the effect of phosphorylation and mutation. *Biophys J* 2005;88:3243–3251.
 23. Michel Espinoza-Fonseca L, Kast D, Thomas DD. Molecular dynamics simulations reveal a disorder-to-order transition on phosphorylation of smooth muscle myosin. *Biophys J* 2007;93:2083–2090.
 24. Pullen K, Rajagopal P, Klevit RE, Branchini BR, Reizer J, Saier MH, Scholtz JM, Huffine ME. Phosphorylation of serine-46 in HPr, a key regulatory protein in bacteria, results in stabilization of its solution structure. *Protein Sci* 1995;4:2478–2486.
 25. Smart JL, McCammon JA. Phosphorylation stabilizes the N-termini of α -helices. *Biopolymers* 1999;49:225–233.
 26. Smet C, Sambo A-V, Wieruszkeski J-M, Leroy A, Landrieu I, Bué L, Lippens G. The peptidyl prolyl cis/trans-isomerase pin1 recognizes the phospho-Thr212-Pro213 site on tau†. *Biochemistry* 2004;43:2032–2040.
 27. Case DA, Darden TA, Cheatham TE, III, Simmerling CL, Wang J, Duke RE, Luo R, Walker RC, Zhang W, Merz KM, Roberts B, Hayik S, Roitberg A, Seabra G, Swails J, Goetz AW, Kolossváry I, Wong KF, Paesani F, Vanicek J, Wolf RM, Liu J, Wu X, Brozell SR, Steinbrecher T, Gohlke H, Cai Q, Ye X, Wang J, Hsieh M-J, Cui G, Roe DR, Mathews DH, Seetin MG, Salomon-Ferrer R, Sagui C, Babin V, Luchko T, Gusarov S, Kovalenko A, Kollman PA. AMBER 12. University of California, San Francisco; 2012.
 28. Hornak V, Abel R, Okur A, Strockbine B, Roitberg A, Simmerling C. Comparison of multiple Amber force fields and development of improved protein backbone parameters. *Proteins* 2006;65:712–725.
 29. Joung IS, Cheatham TE. Determination of alkali and halide monovalent ion parameters for use in explicitly solvated biomolecular simulations. *J Phys Chem B* 2008;112:9020–9041.
 30. Joung IS. Molecular dynamics simulations of the dynamic and energetic properties of alkali and halide ions using water-model-specific ion parameters. *J Phys Chem B* 2009;113:13279.
 31. Steinbrecher T. Revised AMBER parameters for bioorganic phosphates. *J Chem Theory Comput* 2012;8:4405.
 32. Jorgensen WL, Chandrasekhar J, Madura JD, Impey RW, Klein ML. Comparison of simple potential functions for simulating liquid water. *J Chem Phys* 1983;79:926–935.
 33. Darden T, York D, Pedersen L. Particle mesh Ewald: an N [center-dot] log(N) method for Ewald sums in large systems. *J Chem Phys* 1993;98:10089–10092.
 34. Robustelli P, Kohlhoff K, Cavalli A, Vendruscolo M. Using NMR chemical shifts as structural restraints in molecular dynamics simulations of proteins. *Structure* 2010;18:923–933.
 35. Kosol S, Contreras-Martos S, Cedeño C, Tompa P. Structural characterization of intrinsically disordered proteins by NMR spectroscopy. *Molecules* 2013;18:10802–10828.
 36. Kabsch W, Sander C. Dictionary of protein secondary structure: pattern recognition of hydrogen-bonded and geometrical features. *Biopolymers* 1983;22:60.
 37. van der Spoel D, Lindahl E, Hess B, van Buuren A, Apol E, Meulenhoff P, Tieleman D, Sijbers A, Feenstra K, van Drunen R, Berendsen H. Gromacs User Manual version 4.5.4. 2010.
 38. Mansiaux Y, Joseph AP, Gelly J-C, de Brevern AG. Assignment of polyproline II conformation and analysis of sequence – structure relationship. *PLoS One* 2011;6:e18401.
 39. Daura X, Gademann K, Jaun B, Seebach D, van Gunsteren WF, Mark AE. Peptide folding: when simulation meets experiment. *Angew Chem Int Ed* 1999;38:236–240.
 40. Meng E, Pettersen E, Couch G, Huang C, Ferrin T. Tools for integrated sequence-structure analysis with UCSF Chimera. *BMC Bioinformatics* 2006;7:339.
 41. Trabuco L, Villa E. Salt Bridges Plugin. 1.1. Illinois: University of Illinois; 2006.
 42. Humphrey W, Dalke A, Schulten K. VMD: Visual molecular dynamics. *J Mol Graph* 1996;14:33–38.
 43. Rojas Quijano FA, Morrow D, Wise BM, Brancia FL, Goux WJ. Prediction of nucleating sequences from amyloidogenic propensities of tau-related peptides†. *Biochemistry* 2006;45:4638–4652.
 44. Mukrasch MD, Biernat J, von Bergen M, Griesinger C, Mandelkow E, Zweckstetter M. Sites of tau important for aggregation populate β -structure and bind to microtubules and polyanions. *J Biol Chem* 2005;280:24978–24986.
 45. Tompa P, Fersht A. Structure of IDPs. *Structure and Function of Intrinsically Disordered Proteins*. Boca Raton, FL, USA: Chapman and Hall/CRC; 2009. p 121–142.